arXiv:1207.5695v1 [nucl-th] 24 Jul 2012

Microscopic two-nucleon overlaps and knockout reactions from ^{12}C

E. C. Simpson,[1] P. Navrátil,[2] R. Roth,[3] and J. A. Tostevin[1, 4]

[1]*Department of Physics, Faculty of Engineering and Physical Sciences,*
University of Surrey, Guildford, Surrey GU2 7XH, United Kingdom
[2]*TRIUMF, 4004 Wesbrook Mall, Vancouver, British Columbia, V6T2A3, Canada*
[3]*Institut für Kernphysik, Technische Universität Darmstadt, 64289 Darmstadt, Germany*
[4]*National Superconducting Cyclotron Laboratory, Michigan State University, East Lansing, Michigan 48824, USA*

(Dated: July 25, 2012)

The nuclear structure dependence of direct reactions that remove a pair of like or unlike nucleons from a fast ^{12}C projectile beam are considered. Specifically, we study the differences in the two-nucleon correlations present and the predicted removal cross sections when using p-shell shell-model and multi-$\hbar\omega$ no-core shell-model (NCSM) descriptions of the two-nucleon overlaps for the transitions to the mass A=10 projectile residues. The NCSM calculations use modern chiral two-nucleon and three-nucleon (NN+3N) interactions. The np-removal cross sections to low-lying T=0, ^{10}B final states are enhanced when using the NCSM two-nucleon amplitudes. The calculated absolute and relative partial cross sections to the low energy ^{10}B final states show a significant sensitivity to the interactions used, suggesting that assessments of the overlap functions for these transitions and confirmations of their structure could be made using final-state-exclusive measurements of the np-removal cross sections and the associated momentum distributions of the forward travelling projectile-like residues.

PACS numbers: 24.50.+g, 25.70.Mn, 21.10.Pc

I. INTRODUCTION

Properties of the wave functions of pairs of nucleons in a mass $A+2$ projectile can be probed using sudden two-nucleon removal reactions, that exploit fast, surface-grazing collisions of the projectile with a light target nucleus. The sensitivity is to the wave functions of the nucleons at and near the surface of the projectile. When combined with γ-decay spectroscopy, partial cross sections of populated final-states in the mass A reaction residues can be determined. This direct reaction mechanism, its cross sections, and their distributions with the momenta of the forward travelling residues, are now being exploited as a spectroscopic tool in studies of the evolution of nucleon single-particle structure near the Fermi surfaces of some of the most exotic nuclei; see for example Refs. [1–3] and citations therein. The reaction observables used are, currently, inclusive with respect to the final states of both the removed nucleons and of the struck light target nucleus. More exclusive measurements, e.g. of the light charged fragments in the final-state, may in the future provide additional probes of the projectile structure [4].

A detailed discussion of the two-nucleon removal reaction mechanism, its eikonal reaction-dynamical description, and the cross sections and their momentum distributions, in the case of high-energy two-nucleon removal from ^{12}C, was presented in Ref. [5]. A feature of this model description is that the removal cross sections involve only elastic interactions of the projectile residues with the target but sums of contributions from both elastic and inelastic interactions of one or both nucleons with the target [6]. New data, for the sd-shell nucleus ^{28}Mg and the ^{28}Mg$(-2$p$)$ reaction, have quantified these different contributions experimentally [7], and have confirmed that the relative importance of these different processes to the cross sections are consistent with the predictions of the eikonal dynamical model. This has provided an important additional test of the reaction model. In the earlier work for ^{12}C [5], the theoretical comparisons used the sums of these removal contributions and p-shell ($0\hbar\omega$ shell-model) structure calculations were used to construct the required $\langle ^{10}\mathrm{X}(J^{\pi}_{f},T)|^{12}\mathrm{C}\rangle$ two-nucleon overlaps. The PJT [8] and the WBP [9] shell-model effective-interaction Hamiltonians were used.

Key elements of that analysis are also relevant here:

(i) The reaction is geometrically selective [10] and the two-nucleon removal cross sections will be enhanced if the projectile ground-state has components with pairs of nucleons with strong spatial correlations (localization).

(ii) The available experimental cross section data, from high-energy primary-beam measurements, are inclusive with respect to the populated bound states of the residues following np, nn and pp removal [11, 12]. The data, at three energies, reveal a significant enhancement of the ratio of unlike-pair yields, σ_{-np}, to those for the like-nucleon pairs, σ_{-nn} and σ_{-pp}. This enhancement is significantly greater than that expected based simply on the numbers of available 2N-pair combinations (i.e. a factor of 8/3). For example, the experimental $\sigma_{-np}:\sigma_{-nn}$ ratio was 8.54 for the data set with a ^{12}C beam of energy 2.1 GeV per nucleon. Some (but not all) of this enhancement could be explained as due to the pair-correlations already generated in $0\hbar\omega$ p-shell-model overlap functions and because a larger fraction of the nn-removal strength leads to unbound ^{10}C final states. However, the experimental σ_{-np} remained factors of 1.45 to 2.2 larger than the theoretical model calculations for the three available data sets [11, 12]. Table I, reproduced from Ref. [5], shows both the p-shell-model results and data.

(iii) The shapes and widths of the reaction residues' momentum distributions have both diagnostic and spectroscopic value, being indicative of the total angular momentum, I, the total orbital angular momentum L, and hence, with $(LS)I$ coupling, also the total spin S carried by the removed nucleon pair [14].

(iv) The calculated cross sections for the T=1 states common to all three residues, namely the first 0^+ and 2^+ states, are essentially equal. Minor differences in the calculations arise from the small differences in the empirical separation energies for each system. Unlike the np-removal case, these calculated inclusive T=1 cross sections were reasonably consistent with and were fractionally larger than the data values for σ_{-nn} and σ_{-pp}, suggesting that the deficit in the theoretical cross sections in the np channel reflects, primarily, a failure of our description of the overlaps $\langle {}^{10}\mathrm{B}(J^\pi_f, T=0)|{}^{12}\mathrm{C}\rangle$ for the transitions to the T=0, ^{10}B final states.

Here we exploit the eikonal reaction model in the isospin formalism [6, 10, 15] for the removal of the like (T=1) and unlike (T=0,1) pairs of nucleons from ^{12}C. In particular, we will investigate the effect on reaction observables when using *ab-initio* multi-$\hbar\omega$ no-core shell-model (NCSM) descriptions for the two-nucleon overlaps. We contrast these with the earlier $0\hbar\omega$ p-shell shell-model results of Ref. [5]. We discuss the np and nn removal channels to ^{10}B and ^{10}C. These channels share the same $T=1$, 0^+_1 and 2^+_1 final states, see e.g. Fig. 1, whereas the pp channel contains two additional $T=1$ states.

In Section II we reiterate some specific features of the reaction description for ^{12}C projectiles. The necessary formalism has been presented elsewhere [6, 10] to which readers are referred. We follow the notations used in these earlier works. The chiral effective field theory (EFT) two- and three-nucleon (NN+3N) interactions and the microscopic no-core shell-model (NCSM) calculations used to construct the improved overlap functions will be discussed in section III. These include calculations in which the chiral 3N interaction is switched off in an attempt to understand the impact on observables of these 3N interaction terms in the starting Hamiltonian. The new results and predictions for ^{12}C reaction observables are analyzed in section IV and a summary is presented in section V.

II. CARBON-INDUCED REACTIONS

Consideration of two-nucleon removal from ^{12}C is valuable given the availability of both conventional shell-model and ab-initio NCSM structure descriptions. The residual nuclei ^{10}C, ^{10}B (and ^{10}Be) were also extensively studied and so establish a valuable benchmark. In addition, the existing experimental cross section measurements [11, 12], although inclusive with respect to the residue final states, have relatively small quoted uncertainty and were taken at high energies where the eikonal model description of the reaction dynamics is most reliable. These data were obtained for reactions of a carbon beam and carbon target at 250, 1050 and 2100 MeV per nucleon incident energies. As mentioned above, these data (and related data for other light projectile nuclei) show a significant enhancement in their T=0,1, np-removal production cross sections over those with T=1, the nn and pp removal cases (see e.g. Table I). This observed enhancement is of particular interest as a potential signal and a measure of strong np-correlations at the nuclear surface.

The primary motivation for the present study is the implementation and first assessment of improved microscopic descriptions of the two-nucleon overlap functions and their implications for np-correlations and the calculated reaction yields and observables. The relevant final states of the A=10 residual nuclei and their spins and isospins are shown in Fig. 1. The known spectrum of low-lying states in ^{10}B also contains several negative parity states. These are not expected to be populated in the two-nucleon removal reaction mechanism. More exclusive measurements would be needed to confirm this expectation.

The isospin formalism developed in Refs. [6, 10] is used here. The description of the reaction and the parameters used for the ^{12}C and mass A=10 residue densities, etc.

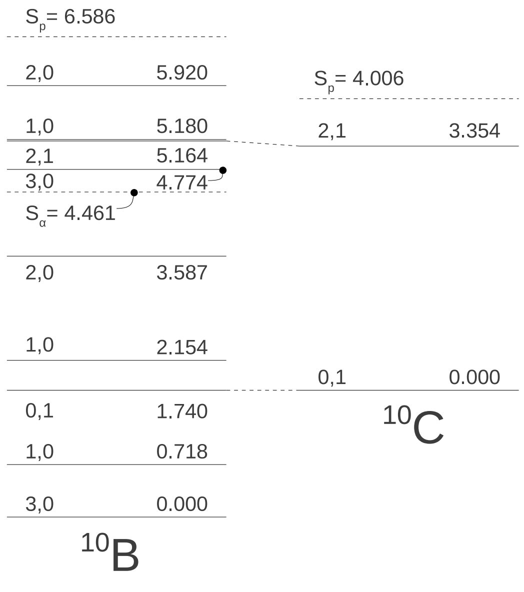

FIG. 1. States of the mass $A=10$ residues populated in the two-nucleon removal reactions considered. The spin and isospin labels (J_f,T) are indicated. All states included are of positive parity. Levels assumed to be part of the isospin multiplet are connected by dashed lines. The lowest particle thresholds are also indicated. States above the α-particle threshold in ^{10}B are expected to decay via α emission, with the exception of the 5.164 MeV, T=1, $J^\pi_f=2^+$ state which has an 84% γ-decay branch.

TABLE I. Calculated and experimental cross sections for two-nucleon removals from ^{12}C, for projectile energies of 250, 1050 and 2100 MeV per nucleon, from [5]. All cross sections are in mb. The calculations use p-shell shell-model wave functions from the WBP effective interaction.

Energy	^{10}Be			^{10}C			^{10}B		
MeV/u	σ_{-2N}	σ_{exp}	$\sigma_{exp}/\sigma_{-2N}$	σ_{-2N}	σ_{exp}	$\sigma_{exp}/\sigma_{-2N}$	σ_{-2N}	σ_{exp}	$\sigma_{exp}/\sigma_{-2N}$
250 [11]	7.48	5.88±9.70	0.79±1.30	5.80	5.33±0.81	0.92±0.14	21.57	47.50±2.42	2.20±0.11
1050 [12]	6.62	5.30±0.30	0.80±0.05	5.13	4.44±0.24	0.87±0.05	19.27	27.90±2.20	1.45±0.11
2100 [12]	6.52	5.81±0.29	0.89±0.04	5.04	4.11±0.22	0.82±0.04	19.02	35.10±3.40	1.84±0.18

are the same as were discussed and tabulated in Ref. [5]. The key approximations were as follows: (a) The removal of nucleons is sudden, their co-ordinates frozen during the short timescale of the relativistic, surface-grazing reactions. (b) The no-recoil (heavy residue) approximation is made [6]. The inclusion of core recoil affects only the diffractive-stripping terms of the reaction mechanism whose contributions are a significantly smaller fraction of the cross section (≈30%) than the two-nucleon stripping terms, for which recoil is not an issue. Thus, recoil can play, at most, a minor role on computed cross sections. It is, in any case, the fractional changes of the cross sections between the NCSM and the p-shell calculations, and between T=0 and T=1 configurations that are of most interest and significance to this work.

The primary difference here is a now considerably-extended set of two-nucleon amplitudes (TNA) C_α^{IT} arising from the multi-shell set of available 2N-configurations $\alpha \equiv [\beta_1, \beta_2]$. Here the index $\beta = (n\ell j)$ denotes the spherical quantum numbers of each active single-particle state in the model space. We evaluate the cross sections for transitions from the projectile initial (ground) state i, with spin (J_i, M_i), to particular residue final states f, with (J_f, M_f). The all-important two-nucleon overlap function for removal of two nucleons 1 and 2 is

$$\Psi_i^{(F)} = \sum_{I\mu T\alpha} C_\alpha^{IT}(I\mu J_f M_f|J_i M_i) \\ (T\tau T_f\tau_f|T_i\tau_i)\,[\overline{\psi_{\beta_1}(1)\otimes\psi_{\beta_2}(2)}]^{T\tau}_{I\mu}\ . \qquad (1)$$

Here J_i^π=0^+ and thus J_f=I, the 2N total angular momentum. We discuss later the use of Woods-Saxon or harmonic oscillator radial functions for the single-particle orbitals ψ_β. The 2N correlations under discussion arise in Eq. (1) from: (a) somewhat trivially, the antisymmetry and angular momentum coupling of nucleon pairs, and (b) the possible coherent pair-enhancement arising from the weights and phases of the TNA that contribute to each J_f final state. The latter and their sensitivity to: (i) the NN+3N effective interactions used, and (ii) the NCSM model-space dimensions, are studied here.

Importantly, unlike the earlier p-shell-only analysis, the NCSM wave functions and overlaps now include active single-particle orbitals of both parities, including up to $N_{max} = 6$ major oscillator shells. The angular correlation function of the two nucleons thus contains both even and odd Legendre polynomial terms in the angular separations of the two nucleons [14, 16] with the likelihood of a greater spatial localization of pairs at the nuclear surface. The degree of such increased correlations is discussed further in the results section where we also show the two-nucleon joint-position probabilities in the impact parameter plane, $\mathcal{P}_{J_f}(\boldsymbol{s}_1, \boldsymbol{s}_2)$, as were defined in Ref. [14]. These display the two-nucleon spatial correlations as delivered by the projectiles and as are seen by the target nucleus that induces the reaction.

Nucleon removal may occur via either elastic (diffraction) or inelastic (stripping) interactions of nucleons with the target nucleus, the former leaving the target in its ground state. The latter lead to cross section contributions that are inclusive with respect to all other target final states. Two-nucleon removal events can involve: (a) both nucleons making inelastic collisions with the target, (b) there being one inelastic and one elastic collision, or (c) both nucleons suffering elastic collisions. Events (b), referred to as diffraction-stripping, are identified in the reaction's absorption cross section but require a projection-off bound states for the elastically interacting nucleon (for details see Refs. [6, 10]). When truncated basis, single major shell, shell-model calculations have been used to generate the TNA, all active single-particle orbits in the shell were included in this projection operator. Here, when using the NCSM calculations in a very large basis, we have limited the projection to the 0p-shell orbitals, as being the appropriate bound states set. Purely elastic 2N-removal events (c) were estimated, as previously [6], from the stripping and diffractive-stripping cross sections. Typically, they contribute to the cross sections at the level of $< 5\%$.

The absorptive eikonal S-matrices, that largely determine the volume of the two-nucleon overlap function that is sampled in the reaction, were calculated by folding the target, nucleon, and reaction residue point-nucleon densities with a zero-range effective nucleon-nucleon interaction. Further details may be found in Ref. [5]. Our primary interest is in the np removal cross sections. Since both the 0_1^+ and 2_1^+ $T = 1$ states are populated in both ^{10}B and ^{10}C we may also extract the cross section for the nn channel. Very minor differences in these partial cross sections will arise from (a) the use of a ^{10}B rather than a ^{10}C S-matrix, and (b) from the small binding energy differences. The latter are not accounted for in the present calculations where harmonic oscillator radial wave functions are used.

III. NN+3N INTERACTIONS AND OVERLAPS

The p-shell ($0\hbar\omega$) shell-model calculations and overlaps were described in Ref. [5] and were computed using the code OXBASH [13]. For the present work, a series of no-core-shell-model calculations, each for a given number of major oscillator shells, N_{max} =0, 2, 4 or 6, were carried out using two chiral EFT NN+3N interaction choices, denoted NCSM1 and NCSM2 in the following.

The calculations used interactions derived within the chiral effective field theory (EFT) approach. In particular, the chiral N^3LO NN interaction of Ref. [19, 20] was used with or without the chiral N^2LO 3N interaction [21] in the local form of Ref. [22]. These interactions were softened by the similarity renormalization group (SRG) technique [23–25], where a unitary transformation is used to suppress the off-diagonal matrix elements (controlled by a parameter Λ). The SRG interaction induces higher-body interaction terms. These induced terms were kept up to the three-body level. It has been shown [26, 27] that four- and higher-body terms are negligible for light nuclei although some evidence for four-body induced terms was observed in ^{12}C calculations with one of the interactions used here (NCSM2) [27]. In NCSM1 the NN+3N Hamiltonian used a 3N cutoff of 400 MeV and used parameters fitted to the ^{3}H lifetime and the ^{4}He binding energy [28]. In NCSM2 the 3N cutoff was 500 MeV and the parameters were fitted to the lifetime and binding energy of ^{3}H [29]. In both cases the SRG was carried out using Λ=1.7 fm^{-1}, although the NCSM2 calculations were also performed with Λ=1.88 fm^{-1} to verify the SRG-Λ independence, i.e., to confirm the unitarity of the SRG transformation. The subsequent NCSM calculations used an harmonic oscillator (HO) basis with an angular frequency $\hbar\omega$=16 MeV. The mass-dependent parameterizations of the oscillator frequency $\hbar\omega = 45A^{-1/3} - 25A^{-2/3}$, agreeing with charge radius observations, suggest a value of $\hbar\omega$=14.9 MeV [31], in reasonable agreement with the value used here.

In the case of the NCSM2 parameterization, the calculations were also repeated, and denoted as NCSM3, when the chiral 3N interaction in the starting Hamiltonian was switched off, but with the SRG-induced 3N effects (with Λ=1.7 fm^{-1}) included. Again, the HO frequency of $\hbar\omega$=16 MeV was employed. Using these NCSM3 TNA we can make a first assessment of the impact on calculations/observables of the inclusion, or not, of the chiral 3N interaction in the starting Hamiltonian.

It should be noted that the ^{10}B structure poses a particular challenge to *ab initio* calculations. In particular, it had been observed that standard accurate NN potentials predict incorrectly the ground-state of ^{10}B to be 1^+0, instead of the experimental 3^+0. The present calculations with the chiral N^3LO NN potential (NCSM3) suffer from the same problem. Only after including the chiral N^2LO NNN term, with the 3N cutoff of 500 MeV NCSM2, does one get the correct ground state spin. Interestingly, the weaker chiral N^2LO NNN with the 3N cutoff 400 MeV, NCSM1, fails to invert the 1^+0 and 3^+0 states, also predicting the wrong ^{10}B ground state spin. See Fig. 2 for a comparison of ^{10}B excitation energies from different calculations used in this paper. Also in the figure, the stability of the spectra with respect to the SRG Λ variation and the size of the model space $N_{\rm max}$ is demonstrated for the NCSM2 case. The situation is somewhat reversed in ^{12}C, where the Hamiltonian NCSM2 with the stronger 3N interaction over-binds ^{12}C by several MeV and overcorrects the splitting of the 1^+0 and 4^+0 states [27]. Using the weaker 3N interaction (NCSM1) both the binding energy and excitation energy description improves. Furthermore, this Hamiltonian (NCSM1) also describes the binding energies of oxygen and calcium isotopes [28] very well. The stronger 3N interaction NCSM2, on the other hand, provides a very good description of lighter nuclei ($A \leq 10$), resolving even long-standing analysing power problems in $p-^4$He scattering [30]. These observations suggest that our knowledge of the 3N interaction in particular is incomplete and additional terms, such as those at the N^3LO of the chiral perturbation theory, must be included. Further, the mass region of A=$10-12$ is ideal

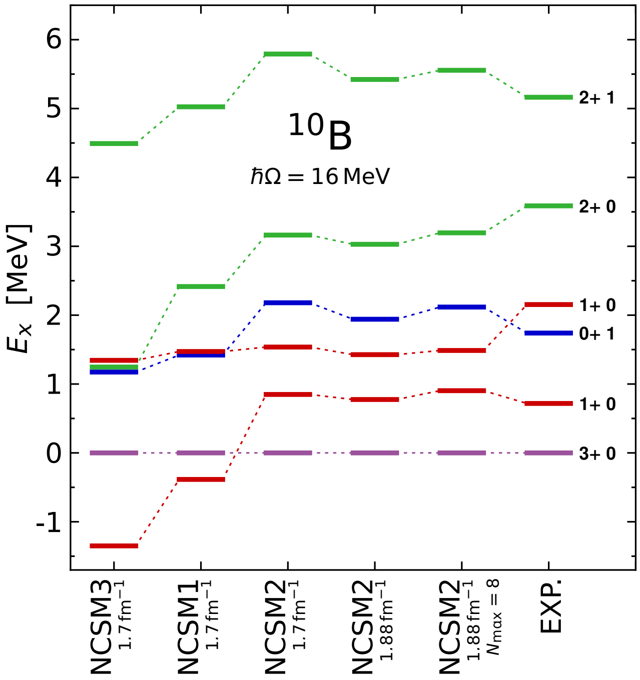

FIG. 2. (Color online) Experimental excitation energies of ^{10}B are compared to the different calculations used in the present work: chiral N^3LO NN (NCSM3), chiral N^3LO NN plus N^2LO 3N with the cutoff of 400 MeV (NCSM1), and chiral N^3LO NN plus N^2LO 3N with the cutoff of 500 MeV (NCSM2). The $N_{\rm max}$=6 space was used in calculations shown in the first four columns. The SRG Λ parameter is indicated. The HO frequency of $\hbar\Omega$=16 MeV was used in all calculations.

to test the details of the nuclear Hamiltonians.

IV. RESULTS

Reaction calculations were carried out using the extended TNA sets derived from the two NN+3N effective interactions outlined in section III, for each of N_{max} =0, 2, 4 and 6, and for the *nn* and *np*-removal channels. In Table II we first show the calculated inclusive cross sections for the *p*-shell WBP and (the most complete) NCSM N_{max} =6 calculations at the three energies of the available data. The NCSM calculations use harmonic oscillator radial form factors with $\hbar\omega$=16 MeV, as used in the NCSM basis. The experimental inclusive cross sections were shown in Table I. We note that when using the PJT *p*-shell effective interaction the inclusive ^{10}B yield at 2.1 GeV per nucleon was 18.73 mb [5], as compared to the 19.02 mb shown in Table II for the WBP case. Thus the two *p*-shell calculations are entirely consistent in this inclusive cross section observable. We note that the *p*-shell-model calculations, taken from [5], use Woods-Saxon radial wave functions when constructing the two-nucleon overlap functions. If $\hbar\omega$=16 MeV oscillator functions are used the calculated cross section is reduced by $\sim 7\%$ for the lowest energy 3^+, and by $< 3\%$ for higher energy states. The smaller changes for the higher residue excitations are due to the absence of any binding energy effect when a single oscillator frequency is used.

The cross sections, now exclusive with respect to the *A*=10 final states, are shown in Table III for the highest energy of 2.1 GeV per nucleon. The two NN+3N NCSM cases (with N_{max} =6) and the WBP case are shown together with the NCSM3 case (i.e. without the chiral 3N interaction in the starting Hamiltonian). In *np*-removal to ^{10}B the cross sections are shown for the six positive parity gamma-decaying final states below the first nucleon threshold. However, the first 2^+, *T*=1 state is known to decay by α-emission with an $I_\alpha = 16\%$ branch. This branching has been accounted for in the inclusive σ_{-2N} values presented. The cross sections for population of the three higher lying *T*=0 states (see Fig. 1) are not included since these states are reported to decay by α-emission (with $I_\alpha = 100\%$). It was assumed that these states do not contribute to the ^{10}B yields.

Table III reveals significant sensitivity of the yields of the low-lying ^{10}B states to the interactions assumed. The ratio of the *T*=0, 1^+_1 to 3^+ ground-state yields is reversed between NCSM1 and NCSM2. The absence of the 3N interaction in the NCSM2 starting Hamiltonian, the NCSM3 case, leads to a quite significantly enhanced ratio of the *T*=0 1^+_1 to 3^+ ground-state cross sections when compared to the full NCSM2 Hamiltonian. To confront these detailed model predictions requires more exclusive measurements with good statistics.

The six contributing ^{10}B partial cross sections are also plotted in Figs. 3, 5 and 6. Fig. 3 shows the calculations, using NCSM1, for N_{max} =0, 2, 4 and 6, and the stabilization and the essential convergence of the calculated partial cross sections (upper panel) and the full-width at half-maximum widths of their momentum distributions (lower panel) with increasing N_{max}. Based on this observed convergence, seen for all of the NCSM cases, we have presented, in the main, only the final N_{max}=6 results. Fig. 4 shows $N_{\rm max} = 6$ NCSM2 calculations for two different SRG Λ values, Λ=1.7 fm^{-1} and Λ=1.88 fm^{-1}. The essential independence of the cross sections and the FWHM on the SRG-Λ confirms the unitarity of the SRG transformation, i.e., we are really investigating predictions of the initial chiral interactions. Based on the results of Ref. [27], the SRG Λ dependence is expected to be even weaker for the NCSM1 and NCSM3 cases. Fig. 5 shows the calculations from the NCSM1, NCSM2 and NCSM3 Hamiltonians, all with N_{max} =6. The significant variations predicted in the widths of the momentum distributions for the different final states and the sensitivity of the *T*=0, ^{10}B final state yields to these effective interactions, are evident. The momentum distribution widths from the NCSM interactions are broadly consistent, and also with those of the conventional truncated-basis *p*-shell model interactions (shown in Fig. 6). They are systematically wider than the latter by $\approx$ 25 MeV/c that we attribute to the incorrect asymptotic of the oscillator wave functions. These similarities reflect the relative insensitivity of the different *LS*-fractions in the overlap to the interactions used. The notable exception is the second $T = 0$, 1^+ excited state, when the width using the NCSM interactions is somewhat wider than that from the conventional shell-model interactions. The comparison of the NN+3N and *p*-shell shell-model results are shown in Fig. 6.

The final-state inclusive cross sections for the NCSM interactions are all larger than those from the truncated-space WBP interaction. All three NCSM interactions result in similar summed cross sections to the lowest two $T = 0$ states, between 16 and 17 mb, but the distribution of this strength between the two states shows significant variations. The cross sections to the $T = 1$, 0^+ state is also larger when using the NCSM interactions with variations between the predictions of the interactions, thus reinforcing the need for final-state-exclusive cross section measurements. The detailed nature of the sensitivity of the TNA, and hence the final-state branching ratios and cross sections, to the details of the interactions is complex, but precise measurements could provide a path to probe this sensitivity and toward constraining the underlying interactions.

The ratios of the theoretical model and experimental cross sections, $R_s(2N) = \sigma_{exp}/\sigma_{th}$ are $R_s(2n) = 0.66$ and $R_s(np) = 1.40$ for the NCSM1 interaction and $R_s(2n) = 0.56$ and $R_s(np) = 1.35$ for NCSM2. Calculations for two-nucleon removal in exotic *sd*-shell isotopes typically overestimate the experimental observations by a factor of two with $R_s(2N) = 0.5$ [6]. As mentioned above, we do not include core recoil and center-of-mass effects for the structure amplitudes, so do not draw specific conclusions

TABLE II. Calculated inclusive cross sections for two nucleon removals from ^{12}C, for projectile energies of 250, 1050 and 2100 MeV per nucleon. All cross sections are in mb. The TNAs used were calculated using the *p*-shell and WBP interaction, and the NSCM1 and NSCM2 NN+3N interactions with N_{max}=6. The experimental cross sections were tabulated in Table I.

Energy	^{10}C			^{10}B		
MeV/u	$\sigma_{-2N}^{\mathrm{WBP}}$	$\sigma_{-2N}^{\mathrm{NCSM1}}$	$\sigma_{-2N}^{\mathrm{NCSM2}}$	$\sigma_{-2N}^{\mathrm{WBP}}$	$\sigma_{-2N}^{\mathrm{NCSM1}}$	$\sigma_{-2N}^{\mathrm{NCSM2}}$
250	5.80	7.10	8.48	21.57	28.19	29.91
1050	5.13	6.31	7.44	19.27	25.26	26.45
2100	5.04	6.22	7.28	19.02	25.00	26.01

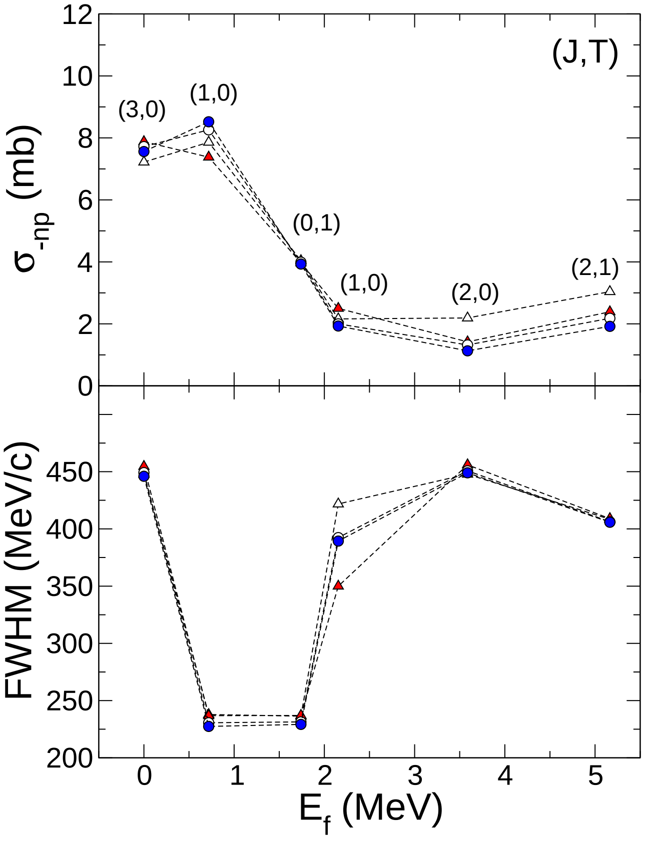

FIG. 3. (Color online) Calculated exclusive cross sections (upper panel) and full width at half maximum (FWHM) widths of the momentum distributions (lower panel) for the ground and γ-decaying final states of the ^{10}B residues, following *np*-removal at 2100 MeV per nucleon. The TNAs used were obtained using the NCSM1 NN+3N starting Hamiltonian (dashed lines). Calculations are for N_{max}=0 (open triangles), 2 (red triangles), 4 (open circles) and 6 (blue circles).

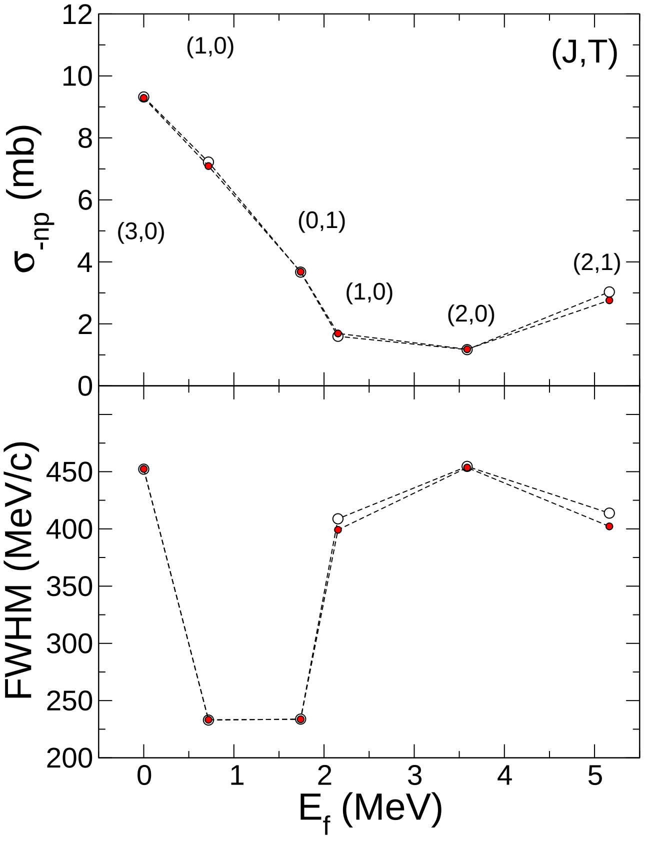

FIG. 4. (Color online) Calculated exclusive cross sections (upper panel) and FWHM widths of the momentum distributions (lower panel) for the ground and γ-decaying final states of the ^{10}B residues, following *np*-removal at 2100 MeV per nucleon. The TNAs used were obtained using the NCSM2 NN+3N starting Hamiltonian (dashed lines). Calculations are for N_{max}=6 with the SRG Λ=1.7 fm^{-1} (open circles) and Λ=1.88 fm^{-1} (red circles).

about these absolute values of $R_s(2N)$. However, both effects should be independent of the reaction channel, and the former will not affect the strongest mechanism, i.e. 2N-stripping.

To consider the impact of the significantly larger model spaces introduced using the NCSM amplitudes, it is meaningful to consider the cross section ratios $\sigma_{-2N}^{WBP}/\sigma_{-2N}^{NCSM}$, i.e., the relative enhancement of a particular channel when moving from the truncated basis WBP to the NCSM interactions. For the NCSM1 interaction, this ratio is 0.81 for the *nn* channel and 0.76 for the *np* channel. The corresponding numbers for the NCSM2 interaction are 0.69 and 0.73. Evidently, the use of the larger basis amplitudes set enhances the cross section.

A significant fraction of these differences results from changes in the *p*-shell amplitudes, as are shown in Ta-

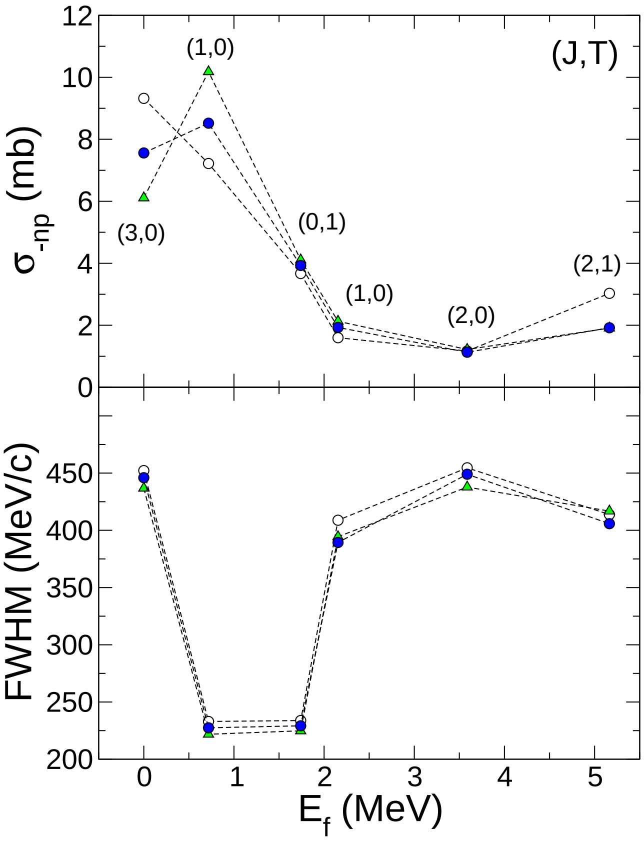

FIG. 5. (Color online) Calculated exclusive cross sections (upper panel) and FWHM widths of the momentum distributions (lower panel) for the ground and γ-decaying final states of the ^{10}B residues, following np-removal at 2100 MeV per nucleon. The TNAs used were obtained using the NCSM1 (blue circles) and NCSM2 (open circles) NN+3N starting Hamiltonians and the NCSM3 (triangles) NN starting Hamiltonian, all for N_{max}=6.

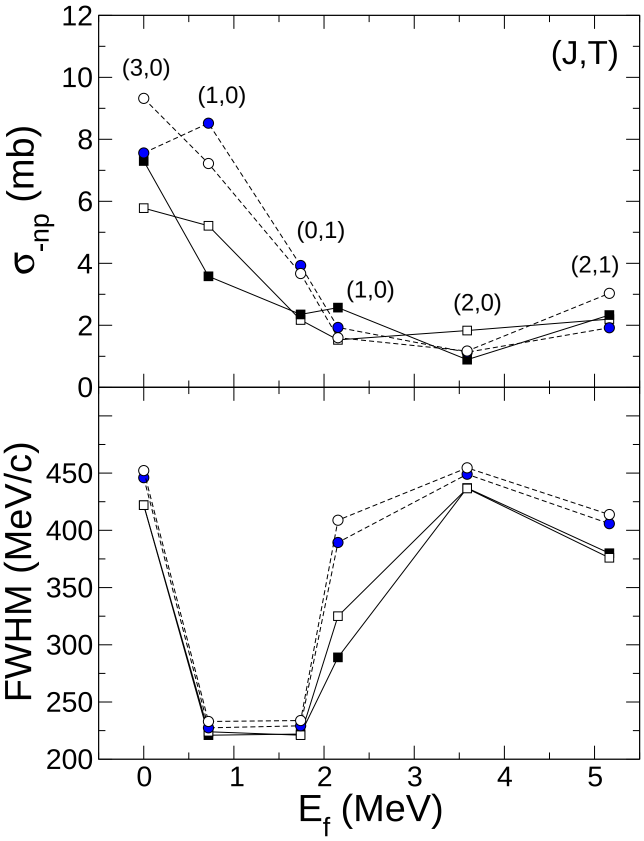

FIG. 6. (Color online) Calculated exclusive cross sections (upper panel) and FWHM widths of the momentum distributions (lower panel) for the ground and γ-decaying final states of the ^{10}B residues, following np-removal at 2100 MeV per nucleon. The TNAs used were obtained using the WBP interaction (solid lines and solid squares), the PJT interaction (solid lines and open squares) shell-model interactions and the NCSM1 (dashed lines blue circles) and NCSM2 (dashed lines and open circles) NN+3N Hamiltonians for N_{max}=6.

ble IV, the simplest case being the 3^+ ground state, where only a single p-shell configuration contributes. The $[0p_{3/2}]^2$ TNA vary, depending on the different interactions, and the magnitude of these p-shell amplitudes is a key factor in the cross section changes observed.

For the two $T=0$, 1^+ states, a mix of p-shell configurations now contribute, with the overall magnitude of the TNA and their relative strengths and phases changing. The relative strengths of the three configurations are broadly consistent across the NCSM interactions, but are different from the truncated-basis WBP interaction. In particular the $[p_{3/2}]^2$ TNA are different, with some apparent shift of strength from the first to the second 1^+ state, when compared to the NCSM interactions. In these cases there is interference between the different configurations that make it less transparent what one expects from the different interactions. Changes in the p-shell configurations will account for a part of the changes in cross sections shown in Table III and the predicted momentum distribution widths for the second 1^+ state, offering a means to discern between the different interactions.

Further enhancement of the cross section may arise from the new couplings to higher major shells. Coupling to major shells of the same parity (odd N) will lead to generic changes to the overall size of the two-nucleon overlap functions and TNA. The TNA due to mixing with major shells of opposite parity (even N) leads to new interference affects that can enhance two-nucleon spatial correlations (see e.g., [16]). For the first 1^+ this can be seen in Fig. 7 for calculations based on the NCSM1 Hamiltonian. The left panel is calculated when retaining only the $0\hbar\omega$ p-shell TNA components from the $N_{max}=6$ NCSM calculation. The right panel includes the full set of NCSM TNA for all major shells. The enhanced spatial correlations presented to the target nucleus from the inclusion of single-particle configurations with opposite parity in the two-nucleon overlap function are evident. The cross sections from these truncated and full TNA sets are 6.09 and 8.52 mb, respectively. Both exceed those of the p-shell shell-model calculations, this being

TABLE III. Like and unlike two-nucleon removal cross sections (in mb) for a ^{12}C projectile incident on a carbon target at 2100 MeV per nucleon. The excitation energies, E_f, of each final state are shown in Fig. 1. The TNAs used were calculated using (a) the $0\hbar\omega$ p-shell-model and WBP interaction, (b) the two NN+3N interactions NCSM1 and NCSM2 (see text), and (c) the NCSM3 Hamiltonian in which the chiral 3N interaction is turned off. Calculations (b) and (c) use the NCSM with $N_{max} = 6$. The sums show the accumulated cross sections that lead to the ground state and the γ-decaying bound excited states of the mass $A = 10$ projectile residues.

Residue	J_f^π	T	$\sigma_{-2N}^{\rm WBP}$	$\sigma_{-2N}^{\rm NCSM1}$	$\sigma_{-2N}^{\rm NCSM2}$	$\sigma_{-2N}^{\rm NCSM3}$
^{10}C	0^+	1	2.30	3.93	3.67	4.11
	2^+	1	2.74	2.29	3.61	2.27
Inclusive			5.04	6.22	7.28	6.38
Experiment				4.11±0.22		
^{10}B	3^+	0	7.30	7.56	9.32	6.11
	1^+	0	3.58	8.52	7.22	10.18
	0^+	1	2.35	3.93	3.67	4.11
	1^+	0	2.57	1.93	1.60	2.13
	2^+	0	0.89	1.13	1.17	1.22
	2^{+a}	1	2.33	1.92	3.03	1.91
Inclusive			19.02	25.00	26.01	25.66
Experiment				35.10±3.40		

[a] state decays by α emission with a 16% α-branch.

TABLE IV. p-shell two-nucleon amplitudes for the WBP, NCSM1, NCSM2 and NCSM3 interactions.

Interaction	(J^π, T)	$[p_{1/2}]^2$	$[p_{1/2}][p_{3/2}]$	$[p_{3/2}]^2$
WBP	$(3_1^+, 0)$	-	-	1.976
	$(1_1^+, 0)$	-0.011	0.979	0.699
	$(1_2^+, 0)$	0.363	0.229	-1.134
NCSM1	$(3_1^+, 0)$	-	-	1.913
	$(1_1^+, 0)$	-0.220	1.034	1.197
	$(1_2^+, 0)$	0.611	0.376	-0.835
NCSM2	$(3_1^+, 0)$	-	-	2.213
	$(1_1^+, 0)$	-0.255	0.863	1.307
	$(1_2^+, 0)$	0.470	0.500	-0.814
NCSM3	$(3_1^+, 0)$	-	-	1.644
	$(1_1^+, 0)$	-0.224	1.137	1.205
	$(1_2^+, 0)$	0.740	0.332	-0.719

3.58 mb for the WBP interaction TNA.

For both NCSM1 and NCSM2 the enhancement of the np removal cross sections relative to the WBP calculations is larger than that for the like-nucleon, nn, removal cross section. However, the difference in this ratio is relatively small. Despite the larger np removal cross section obtained, some underestimation of the experimental np channel cross sections still remains. The available data again suggests that there are remaining deficiencies in the $T = 0$ parts of the two-nucleon overlap functions. The yields to specific final states, namely the first 3^+, 1^+ and 0^+ states, suggest a significant sensitivity to the interactions used, requiring input from final-state-exclusive measurements.

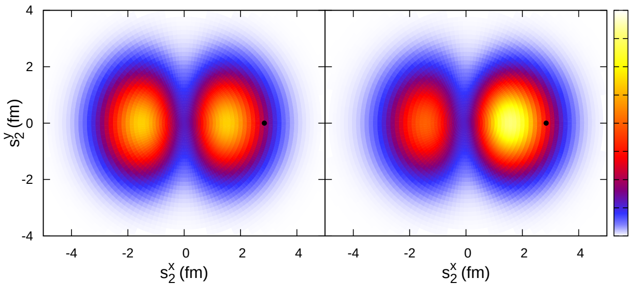

FIG. 7. (Color online) Projected two-nucleon density $\mathcal{P}_f(\boldsymbol{s}_1, \boldsymbol{s}_2)$ from the two-nucleon overlap for the first $T = 0$, 1^+ state, calculated using the NCSM and the NCSM1 Hamiltonian. The contours show the position probability in the impact parameter plane of nucleon 2, $\boldsymbol{s}_2$, when nucleon 1, $\boldsymbol{s}_1$, is at the position indicated by the black point. The left panel is calculated when retaining only the lowest p-shell TNA from the $N_{max} = 6$ calculation. The right panel includes the full set of NCSM TNA for $N_{max} = 6$. The overlap shows the enhanced spatial correlations arising from inclusion of single-particle configurations of opposite parity in the two-nucleon overlap function (see also Fig. 4 of Ref. [14]). The cross sections from these two TNA sets are 6.09 and 8.52 mb, respectively.

V. SUMMARY

We have considered the impact of microscopic, NCSM wave function overlaps on the theoretical cross sections for two-nucleon removal reactions from fast ^{12}C projectiles. Data were available for reactions on a carbon target at beam energies of 250, 1050 and 2100 MeV per nucleon. As found in a previous analysis [5], the np removal cross sections are underestimated by the theoretical model calculations, but do show an enhancement relative to the use of truncated-basis p-shell-model calculations. The cross sections to both $T = 0$ and $T = 1$ states are enhanced, and the use of large-basis NCSM amplitudes does not fully resolve the relative discrepancy between measured np- and nn-removal cross sections.

Further measurements, of final-state-exclusive cross sections and residue momentum distributions, would allow a much more detailed scrutiny and confrontation of the detailed reaction observables predictions, including the identification of any indirect reaction components arising from two-step paths to the final-states. The calculated np-removal cross sections to the T=0, ^{10}B final states were shown to have sensitivity to the different variants of the chiral interactions used; for example, the ratio of the calculated cross sections to the ^{10}B ground $3^+, T = 0$ and first $1^+, T = 0$ excited states. To a lesser degree the first $0^+, T = 1$ state cross section and the branching between the first $T = 1, 0^+$ and 2^+ states was found to depend on the effective interaction. In this case, data for the *nn* and *pp* removal channels would provide useful verification. The momentum distribution of the second $1^+, T = 0$ state also shows a particular sensitivity to the interaction, providing a further useful probe.

The overall conclusion from the present analysis is that the existing residue-final-state-inclusive data suggest that the T=0, *np*-spatial correlations present in the wave functions used are still insufficient. We have shown that new exclusive measurements would offer a means to interrogate these shell-model inputs, in particular for the *np*-channel, $T = 0$ wave functions, and the direct reaction mechanism predictions in considerable detail.

ACKNOWLEDGMENTS

This work was supported by the United Kingdom Science and Technology Facilities Council (STFC) under Grant No. ST/J000051/1 and by the NSERC Grant No. 401945-2011. Computing support for this work came in part from the LLNL institutional Computing Grand Challenge program.

[1] P.G. Hansen and J.A. Tostevin, Ann. Rev. Nucl. Part. Sci. **53**, 219 (2003).
[2] B.A. Brown, P.G. Hansen, B.M. Sherrill and J.A. Tostevin, Phys. Rev. C **65**, 061601 (2002).
[3] J.R. Terry, D. Bazin, B.A. Brown, J. Enders, T. Glasmacher, P.G. Hansen, B.M. Sherrill and J.A. Tostevin, Phys. Rev. C **69**, 054306 (2004).
[4] K. Wimmer *et al.*, *Correlations in intermediate-energy two-proton removal reactions*, submitted (2012).
[5] E.C. Simpson and J.A. Tostevin, Phys. Rev. C **83**, 014605 (2011).
[6] J.A. Tostevin, B.A. Brown, Phys. Rev. C **74**, 064604 (2006).
[7] K. Wimmer *et al.*, Phys. Rev. C **85**, 051603(R) (2012).
[8] R. E. Julies, W. A. Richter and B. A. Brown, South African Jour. Phys. **15**, 35 (1992).
[9] E.K. Warburton, B.A. Brown, Phys. Rev. C **46**, 923 (1992).
[10] E.C. Simpson, J.A. Tostevin, D. Bazin, and A. Gade, Phys. Rev. C **79**, 064621 (2009).
[11] J. M. Kidd, P. J. Lindstrom, H. J. Crawford and G. Woods, Phys. Rev. C **37**, 2613 (1988).
[12] P. J. Lindstrom *et al.*, LBL Report No. LBL3650, 1975 (unpublished); also tabulated in D.L. Olson *et al.*, Phys. Rev. C **28**, 1602 (1983).
[13] B. A. Brown *et al.*, *Oxbash for Windows* (MSU-NSCL report number 1289, 2004).
[14] E.C. Simpson and J.A. Tostevin, Phys. Rev. C **82**, 044616 (2010).
[15] J.A. Tostevin, G. Podolyák, B.A. Brown and P.G. Hansen, Phys. Rev. C **70**, 064602 (2004).
[16] W. T. Pinkston, Phys. Rev. C **29**, 1123 (1984).
[17] E.C. Simpson, J.A. Tostevin, D. Bazin, B.A. Brown and A. Gade, Phys. Rev. Lett. **102**, 132502 (2009).
[18] E.C. Simpson and J.A. Tostevin, Phys. Rev. C **79**, 024616 (2009).
[19] D. R. Entem and R. Machleidt, Phys. Rev. C **68**, 041001 (2003) [nucl-th/0304018].
[20] R. Machleidt and D. R. Entem, Phys. Rept. **503**, 1 (2011) [arXiv:1105.2919 [nucl-th]].
[21] E. Epelbaum, A. Nogga, W. Glockle, H. Kamada, Ulf-G. Meissner and H. Witala, Phys. Rev. C **66**, 064001 (2002) [nucl-th/0208023].
[22] P. Navratil, Few Body Syst. **41**, 117 (2007) [arXiv:0707.4680 [nucl-th]].
[23] S. D. Glazek and K. G. Wilson, Phys. Rev. D **48**, 5863 (1993).
[24] F. Wegner, Ann. Phys. (Leipzig) **3**, 77 (1994).
[25] E. D. Jurgenson, P. Navratil and R. J. Furnstahl, Phys. Rev. Lett. **103**, 082501 (2009) [arXiv:0905.1873 [nucl-th]].
[26] E. D. Jurgenson, P. Navratil and R. J. Furnstahl, Phys. Rev. C **83**, 034301 (2011) [arXiv:1011.4085 [nucl-th]].
[27] R. Roth, J. Langhammer, A. Calci, S. Binder and P. Navratil, Phys. Rev. Lett. **107**, 072501 (2011) [arXiv:1105.3173 [nucl-th]].
[28] R. Roth, S. Binder, K. Vobig, A. Calci, J. Langhammer and P. Navratil, arXiv:1112.0287 [nucl-th].
[29] D. Gazit, S. Quaglioni and P. Navratil, Phys. Rev. Lett. **103**, 102502 (2009) [arXiv:0812.4444 [nucl-th]].
[30] M. Viviani, L. Girlanda, A. Kievsky, L. E. Marcucci and S. Rosati, arXiv:1004.1306 [nucl-th].
[31] J. Blomqvist and A. Molinari, Nucl. Phys. **A106**, 545 (1968).